Journal Pre-proof

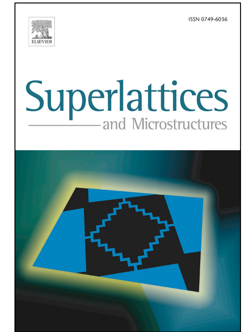

Fabrication and characterization of rare earth (Ce, Gd, and Y) doped ZrO_2 based metal-insulator-semiconductor (MIS) type Schottky barrier diodes

K. Sasikumar, R. Bharathikannan, M. Raja, B. Mohanbabu

PII: S0749-6036(19)31763-X

DOI: https://doi.org/10.1016/j.spmi.2020.106424

Reference: YSPMI 106424

To appear in: *Superlattices and Microstructures*

Received Date: 8 October 2019

Revised Date: 30 December 2019

Accepted Date: 26 January 2020

Please cite this article as: K. Sasikumar, R. Bharathikannan, M. Raja, B. Mohanbabu, Fabrication and characterization of rare earth (Ce, Gd, and Y) doped ZrO_2 based metal-insulator-semiconductor (MIS) type Schottky barrier diodes, *Superlattices and Microstructures* (2020), doi: https://doi.org/10.1016/j.spmi.2020.106424.

This is a PDF file of an article that has undergone enhancements after acceptance, such as the addition of a cover page and metadata, and formatting for readability, but it is not yet the definitive version of record. This version will undergo additional copyediting, typesetting and review before it is published in its final form, but we are providing this version to give early visibility of the article. Please note that, during the production process, errors may be discovered which could affect the content, and all legal disclaimers that apply to the journal pertain.

© 2020 Published by Elsevier Ltd.

Journal Pre-proof

Fabrication and characterization of rare earth (Ce, Gd, and Y) doped ZrO_2 based metal-insulator-semiconductor (MIS) type Schottky barrier diodes

K. Sasikumar[a], R. Bharathikannan[b,*], M. Raja[c], B. Mohanbabu[d]

[a] *Department of Physics, Sri Ramakrishna Engineering College, Coimbatore, Tamil Nadu, 641022, India*

[b] *Department of Physics, Sri Ramakrishna Mission Vidyalaya College of Arts and Science, Coimbatore, Tamil Nadu, 641020, India*

[c] *Department of Physics, Vivekanandha College of Arts & Sciences for Women, Namakkal, Tamil Nadu, 637205, India*

[d] *Department of Electronic Engineering, School of Electronic Science and Technology, Xiamen University, Xiamen, 361005, China*

* Corresponding author: R. Bharathikannan

E-mail: rbk1rys@gmail.com; Phone: +91-422-2692461; Fax: +91-422-2693812

Abstract

The 8 wt.% rare earth (RE = Ce, Gd, and Y) doped zirconium dioxide (ZrO_2) thin films were prepared on glass substrates by spin-coating technique and annealed at 600 ^oC. Also, the RE:ZrO_2 based metal-insulator-semiconductor (MIS) type Schottky barrier diodes were fabricated. X-ray diffraction (XRD) patterns revealed the mixed phase of monoclinic and tetragonal ZrO_2 for the RE:ZrO_2 films, and the pure monoclinic phase for the undoped ZrO_2 film. Because of the doping with RE ions, the crystallite size reduced with the increase of oxygen vacancies. The scanning electron microscopic (SEM) images exhibited the rod-shaped and square-shaped grains for the undoped ZrO_2 and Gd:ZrO_2 thin films, respectively. Elemental compositions were confirmed by the energy dispersive X-ray (EDX) analysis. The UV-vis analysis showed the lower transmittance for the RE:ZrO_2 films with a reduced band gap (E_g). The dc electrical conductivity (σ_{dc}) was increased with the decrease of activation energy (E_a) due to the RE doping. When compared to the Al/undoped ZrO_2/p-Si Schottky barrier diode, the Al/RE:ZrO_2/p-Si showed an improvement in the values of barrier height (Φ_B), ideality factor (n), and series resistance (R_S).

Keywords: ZrO_2; Rare earth; Sol-gel; Schottky barrier diode

1. Introduction

Journal Pre-proof

Schottky barrier diodes (SBDs) are promising candidates in micro/nano electronics technology due to their applications in solar cells, sensors, photodetectors, frequency multipliers, etc. [1-4]. Basically, the SBD consists of a metal deposited over a semiconductor; the structure is known as the metal-semiconductor (MS) structure. Here, the metal electrons can often penetrate into the semiconductor and produce intrinsic states in the semiconductor band gap. These metal-induced gap states (MIGS) create Fermi-level pinning, which results in large contact resistance due to a high Schottky barrier height (Φ_B) [5]. The higher value of Φ_B leads to low reverse saturation current (J_S), on the other hand, it facilitates forward voltage drop (V_F) in the SBD [6]. To solve this issue, an insulating layer is introduced between the metal and semiconductor, which converts the MS type SBD into metal-insulator-semiconductor (MIS) type SBD. The electrical characteristics of the SBD such as barrier height inhomogeneities, the density distribution of interface states (N_{SS}), ideality factor (n), and series resistance (R_S) are affected by some microstructural properties of the insulating layer [7,8]. These properties include crystal phase, crystallite size, grain orientation, atomic stoichiometry, homogeneity, etc. [9-11]. Therefore, in order to improve the overall performance of the SBD, it is essential to control the properties of the insulating layer. This can be achieved by doping of the insulating layer with impurities and thermal annealing [12,13].

Recently, metal-oxide thin films with different dopants have been used as insulating layers in SBDs [14-16]. Among them, zirconium dioxide (ZrO_2) exhibits high dielectric constant (22-25), wide band gap (5.8-7.8 eV), high thermal stability, and good Zr/Si interface [17]. The wide band gap favors to doping with different type of transition and rare earth (RE) metal cations [18,19]. The ZrO_2 have three crystal phases viz. monoclinic (m-ZrO_2 up to 1170 °C), tetragonal (t-ZrO_2 between 1170-2370 °C), and cubic (c-ZrO_2 above 2370 °C) [20]. The RE doped ZrO_2 is well known for its optoelectronic device applications [21-23]. The nature and stoichiometry of RE ions determine the resultant microstructural, optical, and electrical properties of the ZrO_2. Generally, the ionic radius of RE is rather higher than that of the Zr. For instance, when compared to the ionic radius of Zr^{4+} [r = 0.72 Å (m-ZrO_2) and 0.84 Å (t-ZrO_2) with coordination 6 and 8], the RE cations have higher radius [r = 0.87 Å (Ce^{4+}), 0.89 Å (Er^{3+}), 0.90 Å (Y^{3+}), 0.91 Å (Dy^{3+}), 0.94 Å (Gd^{3+}), 1.03 Å (La^{3+})]. When doping with RE ions, they can occupy the substitutional/interstitial sites in the Zr-O host lattice and introduce oxygen vacancies, which are owing to the t-ZrO_2 phase formation [24]. The creation of oxygen vacancies could result in the

Journal Pre-proof

improvement of electrical characteristics of the SBD [25,26]. Many techniques such as sol-gel, chemical vapor deposition, pulsed laser deposition, and sputtering are employed to prepare the metal-oxide films. However, the sol-gel technique offers several advantages such as high purity films at low cost, control over stoichiometry, flexibility for doping, and large coating area [27].

Liu et al. [28] investigated the ZrLaO gate dielectric based MOS capacitor annealed at 850 ^oC. They obtained a low Φ_B of 0.82 eV with the higher reverse current for the Al/ZrLaO/p-Si due to trapped charges. Xiao et al. [29] suggested that the creation of oxygen vacancy improves the leakage current density (1.8×10^{-6} A/cm^2) in the Al/Gd:ZrO_2/Si/Al MIS structure with 15% Gd. Lee et al. [30] fabricated the MOS structures with Y, Gd, Dy, and Ce doped ZrO_2 and the Al/Ce doped ZrO_2/TaN showed limited leakage current due to controlled oxygen vacancies. Chen et al. [31] reported that the Φ_B value of Au/$ZrO_{1.68}$/n-Si/In device (0.47 eV) is lower than the Au/$ZrO_{2.01}$/n-Si/In (0.53 eV) owing to the increase of oxygen vacancies.

By considering the above facts, in the present work, we report the preparation of ZrO_2 thin films with the Ce^{4+}, Gd^{3+}, and Y^{3+} dopant ions using the spin-coating technique. After annealing treatment at 600 ^oC, the microstructural, morphological, optical, and electrical properties of the RE:ZrO_2 films have been studied in detail. Further, the electrical characteristics have been analyzed for the Al/RE:ZrO_2/p-Si SBDs using the thermionic emission theory.

2. Experimental details

2.1 Thin film preparation and MIS Schottky barrier diode fabrication

The precursor solutions were prepared by dissolving 0.2 M of zirconyl chloride octahydrate ($ZrOCl_2.8H_2O$, Sigma Aldrich) in 20 ml of ethanol. The 0.5 g of polyethylene glycol (PEG-6000) and citric acid were added as a surfactant and chelating agent, respectively. These solutions were stirred using magnetic stirrer. After 1 h, 8 wt.% of cerium chloride ($CeCl_3.7H_2O$), yttrium chloride ($YCl_3.6H_2O$), and gadolinium chloride ($GdCl_3.6H_2O$) were separately added into each solution and stirred for 48 h in ambient conditions. The as-prepared sol was spin-coated onto ultrasonically cleaned glass substrates at 3000 rpm for 30 s. Then, the films were dried at 60 ^oC for 10 min and subsequently annealed at 600 ^oC for 1 h. The MIS Schottky barrier diodes were successfully fabricated on p-type silicon (100) substrates. Initially, the substrates were ultrasonically treated with acetone and IPA to remove surface contaminants. In the next step, the substrates were cleaned in piranha solution ($3H_2SO_4$:$1H_2O_2$) and 1% HF solution to remove the

native oxide layer. Finally, the RE doped ZrO_2 films were prepared by spin-coating the sol onto the dried Si substrates followed by annealing at 600 ^oC. An Aluminum target was DC sputtered using a shadow mask to make a Schottky contact (with an area of 0.1256 cm^2) on the film surface. The schematic diagram of the SBD is shown in Fig. 1.

2.2 Characterization techniques

Crystalline properties of the thin films were analyzed by using Bruker AXS D8 advance X-ray diffractometer. The Cu K_α radiation (λ = 1.5406 Å) with a 2θ scan in the range of 20-80° and a step size of 0.02° were employed. The thickness measurement was carried out using Mitutoyo SJ301 stylus profilometer. The morphological characteristics and chemical compositions were examined using JEOL JSM - 6390LV scanning electron microscope and energy dispersive X-ray spectrometer. Optical transmittance of the thin films was investigated with Jasco-V770 UV-vis spectrophotometer in the wavelength range of 200-900 nm. The dc electrical measurement was carried out using the four-point probe set up in the temperature range of 30-210 ^oC with the sweep voltage of 1-10 V. Current density-voltage (J-V) characteristics (in the range of -3 V to +3 V) of the Al/RE:ZrO_2/p-Si SBDs were analyzed by employing the 6517-B Keithley source meter at room temperature.

3. Results and discussion

3.1 Structural analysis

Figure 2 shows the XRD patterns of undoped ZrO_2 and RE:ZrO_2 (RE = Ce, Gd, and Y) thin films coated on Si substrate using the spin-coating technique. The peak located at 69.12^o is correspond to (4 0 0) plane of Silicon substrate. For the undoped ZrO_2 film, diffraction peaks originated at 2θ = 31.22^o, 34.75^o, 38.90^o, 40.03^o, 61.16^o, 76.24^o are indexed as $(1\ 1\ 1)_m$, $(2\ 0\ 0)_m$, $(2\ 1\ 0)_m$, $(-2\ 1\ 1)_m$, $(-2\ 1\ 3)_m$ and $(0\ 3\ 3)_m$ belong to the monoclinic phase of ZrO_2 [JCPDS card no. 65-2357]. The Ce:ZrO_2 film shows peaks at 31.18^o, 36.01^o, 39.74^o, 51.27^o, 60.91^o correspond to $(1\ 1\ 1)_m$, $(-1\ 0\ 2)_m$, $(-1\ 1\ 2)_m$, $(-2\ 2\ 1)_m$, $(1\ 1\ 3)_m$ planes of monoclinic ZrO_2 and a small peak at 34.69^o correspond to $(0\ 0\ 2)_t$ plane of tetragonal phase [JCPDS card no. 78-1807 and 79-1771]. In the case of Gd:ZrO_2 thin film, peaks at 31.06^o, 34.04^o, 38.13^o, 39.02^o, 55.32^o, 66.84^o are assigned to $(1\ 1\ 1)_m$, $(0\ 0\ 2)_m$, $(0\ 1\ 2)_m$, $(0\ 2\ 1)_m$, $(-1\ 1\ 3)_m$, $(-2\ 3\ 1)_m$ planes with monoclinic phase. Also, the peaks observed at 50.86^o, 60.34^o, 72.89^o are originated from $(2\ 0\ 0)_t$, $(2\ 1\ 1)_t$, $(0\ 0\ 4)_t$ planes of the tetragonal phase [JCPDS card no. 80-0966 and 79-1763]. For the Y:ZrO_2 thin

Journal Pre-proof

film, diffraction peaks appeared at 31.11°, 35.81°, 49.44°, 51.20° are attributed to the $(1\ 1\ 1)_m$, $(-1\ 0\ 2)_m$, $(0\ 2\ 2)_m$, $(-2\ 2\ 1)_m$ planes with monoclinic phase and the peaks at 30.14°, 34.77°, 42.78° are assigned to $(1\ 0\ 1)_t$, $(0\ 0\ 2)_t$, $(1\ 0\ 2)_t$ planes of the tetragonal phase [JCPDS card no. 78-1807 and 79-1763]. Doping ZrO_2 lattice with RE ions causes the shift of major (1 1 1) peak towards lower angle. Moreover, any distinguished peaks corresponding to the RE oxides are not observed. The RE doped ZrO_2 films consist of mixed monoclinic and tetragonal phases.

The crystallite size (D) of the undoped ZrO_2 and RE:ZrO_2 thin films was determined from the major (1 1 1) peak using the Scherrer equation [32]:

$$D = \frac{0.89\lambda}{\beta \cos\theta} \tag{1}$$

where λ is the wavelength of CuK_α radiation (0.15406 nm), β is the full-width at half maximum (FWHM), and θ is the peak position. The dislocation density (δ), microstrain (ε), and stacking fault (SF) were determined using the following relations [33,34]:

$$\delta = \frac{1}{D^2} \tag{2}$$

$$\varepsilon = \frac{\beta\cos\theta}{4} \tag{3}$$

$$SF = \left[\frac{2\pi^2}{45(3\tan\theta)^{1/2}}\right]\beta \tag{4}$$

The structural parameters are summarized in Table 1. The D values of undoped ZrO_2, Ce:ZrO_2, Gd:ZrO_2, and Y:ZrO_2 films are calculated to be 6.752 nm, 5.842 nm, 4.640 nm, and 5.775 nm, respectively. It is obvious that the crystallite size decreases with the increase of the ionic radius of dopants. As the RE dopants inhibit the nucleation in the Zr-O lattice due to their larger ionic radius, the crystallite size is reduced [35]. It is noticed that the Gd:ZrO_2 film has smaller crystallites with large defects. The calculated values of δ are 2.193×10^{16}, 2.929×10^{16}, 4.643×10^{16}, and 2.998×10^{16} lines/m^2 for the undoped ZrO_2, Ce:ZrO_2, Gd:ZrO_2, and Y:ZrO_2 thin films, respectively. The increase of crystal defects like vacancies and dislocations is owing to the substitution of RE ions in place of Zr. Since the Ce^{4+} has the same oxidation state as like as Zr^{4+}, it produces minimum defects. But, the Gd^{3+} and Y^{3+} ions possess the oxidation state of +3. Therefore, they create oxygen vacancies in the host lattice in order to balance the charge compensation [36]. These vacancies increase the microstrain in the RE:ZrO_2 films and also lead to the formation of tetragonal phase [37,38].

3.2 Morphological analysis

Figure 3 (a-d) shows the SEM images of undoped ZrO_2 and RE:ZrO_2 thin films. The prepared films exhibit a continuous and smooth surface. In Fig. 3 (a), the undoped ZrO_2 film shows the larger rod-shaped grains. From Fig. 3 (b), it is evident that the grain distribution is uniform throughout the surface of Ce:ZrO_2 film. Figure 3 (c) shows the presence of square-shaped grains in the Gd:ZrO_2 film. The Y:ZrO_2 film surface exhibits closely packed grains with micro-cracks as well as randomly distributed pores, as shown in Fig. 3 (d). The growth of larger grains is owing to the agglomeration of nano-sized crystallites during the annealing treatment at 600 ^oC.

3.3 Energy dispersive X-ray analysis

The EDX spectra of the undoped ZrO_2 and RE:ZrO_2 thin films are presented in Fig. 4 (a-d). The spectral analysis shows that the Zr and O elements are present in all the prepared films. Also, the EDX patterns of Ce:ZrO_2, Gd:ZrO_2, and Y:ZrO_2 thin films confirm the incorporation of RE ions into the ZrO_2 lattice. The elemental compositions are shown in the inset of Fig. 4(a-d). It is evident that the atomic percentage (at.%) of oxygen is lower for the Gd:ZrO_2 thin film, which suggests the presence of oxygen vacancies.

Journal Pre-proof

3.4 Optical studies

Optical transmittance spectra of the undoped ZrO_2 and RE:ZrO_2 thin films recorded at room temperature are shown in Fig. 5. The average transmittance is about 75% in the visible region for the undoped ZrO_2 film. The RE:ZrO_2 thin films exhibit relatively lower transmittance and the average values are 65 %, 70 %, and 60 % for the Ce:ZrO_2, Gd:ZrO_2, and Y:ZrO_2 films, respectively. The transmittance decreases due to the grain boundaries and defects produced by the dopant ions [39]. For all the prepared films, the transmittance increases sharply at 200 nm in the UV region. Beyond 350 nm, the transmittance increases continuously for the Gd:ZrO_2 and Y:ZrO_2 films, and extends throughout the visible region. Meanwhile, the transmittance decreases for the Ce:ZrO_2 thin film.

The optical band gap (E_g) for the direct allowed transition is calculated from the Tauc equation [40]:

$$(\alpha h\nu)^2 = B(h\nu - E_g) \tag{5}$$

where α is the absorption coefficient, $h\nu$ is the photon energy, and B is the constant. The value of α is calculated using the relation [41]:

$$\alpha = \left(\frac{1}{d}\right) \ln\left(\frac{1}{T}\right) \tag{6}$$

where d is the film thickness and T is the transmittance. The band gap is determined by extrapolating the linear portion of the Tauc plot to the x-axis, as illustrated in Fig. 6. As shown in Table 2, the E_g values are 5.64 eV, 5.53 eV, 5.25 eV, and 5.38 eV for the undoped ZrO_2, Ce:ZrO_2, Gd:ZrO_2, and Y:ZrO_2 thin films, respectively. The decrease of band gap is due to the defect states introduced into the forbidden band by doping ZrO_2 with the RE ions [42].

3.5 DC electrical characterization

The dc electrical conductivity (σ_{dc}) was calculated for the undoped ZrO_2 and RE:ZrO_2 thin films using the following equation [43]:

$$\sigma_{dc} = \frac{t}{RA} \tag{7}$$

where t is the inter-probe distance, R is the resistance of the film, and A is the area of the film. As shown in Fig. 7, the undoped ZrO_2 and RE:ZrO_2 thin films exhibit an increase in conductivity with the raise in temperature (30-210 ^oC). This increment is due to the thermally excited free charge carriers hopping from one localized state to another state [44,45]. The average value of 5.827×10^{-12} S/cm is observed for the undoped ZrO_2 film.

Besides, the RE:ZrO_2 thin films possess higher conductivity than the undoped ZrO_2. The Ce:ZrO_2 and Y:ZrO_2 films have σ_{dc} in the order of 10^{-12} S/cm, meanwhile, the highest value of 1.172×10^{-11} S/cm is observed for the Gd:ZrO_2 film. The Gd ions (Gd^{3+}) occupy the substitutional sites in the Zr-O host lattice and lead to the release of free-charge carriers, which are owing to the increase of conductivity. These ions act as scattering centers and induce more vacancy related defects, which also support to the enhancement of conductivity in the Gd:ZrO_2 film. Since the Ce^{4+} and Zr^{4+} have the same oxidation states, the oxygen defects produced by the Ce^{4+} ions are less and therefore, the Ce:ZrO_2 film shows the lower conductivity. The activation energy (E_a) and conductivity (σ_{dc}) are related by the Arrhenius equation as follows [46]:

$$\sigma_{dc} = \sigma_o \exp\left(\frac{-E_a}{k_B T}\right) \tag{8}$$

where k_B is the Boltzmann constant and T is the absolute temperature. The pre-exponential factor (σ_o) represents the number of vacancies, which is determined from the straight line intercept on the y-axis of the Arrhenius plot. Figure 8 shows the plot of ln(σ_{dc}) vs. (1/T) for the undoped ZrO_2

Journal Pre-proof

and RE doped ZrO_2 thin films. The calculated value of E_a is found to be in the range of 0.068 to 0.093 eV. The σ_{dc} and E_a values are listed in Table 3.

3.6 Current density-voltage (J-V) measurement

Based on the thermionic emission theory, the forward current through the SBD and the applied bias (V > 3kT/q) are related as [47]:

$$J = J_S \left[\exp\left(\frac{qV}{nkT}\right) - 1\right] \quad (9)$$

where J_S is the saturation current density, q is the electric charge, n is the ideality factor, k is the Boltzmann constant, and T is the absolute temperature. The saturation current density (J_S), ideality factor (n), and barrier height (Φ_B) can be determined by using the relations [48]:

$$J_S = \frac{I_S}{A} = A^* T^2 \exp\left[\frac{-q\Phi_B}{kT}\right] \quad (10)$$

where A is the area of Schottky contact and A* is the effective Richardson constant (32 A/cm^2K^2 for p-Si).

$$n = \frac{q}{kT}\frac{dV}{d(\ln J)} \quad (11)$$

$$\Phi_B = \frac{kT}{q}\ln\left[\frac{A^* T^2}{J_S}\right] \quad (12)$$

The J_S, n values are calculated by extrapolating the linear portion of the ln(J)-V plot toward V = 0 and slope of the linear portion of the ln(J)-V plot, respectively. The Cheung's function is used to determine the series resistance (R_S) as follows [49]:

$$\frac{dV}{d\ln(J)} = JR_S + \frac{nkT}{q} \quad (13)$$

The energy band diagram of Al/RE:ZrO_2/p-Si SBD is depicted in Fig. 10. When a positive bias is applied on the p-Si relative to the metal, the electrons from Al metal flow out through the RE:ZrO_2 insulating layer and create ionized acceptors above the valence band in p-Si. Meanwhile, holes (majority carriers) move from the valence band into metal and hence current flows in SBD. The forward and reverse bias semi-logarithmic J-V characteristics of the Al/RE:ZrO_2/p-Si Schottky barrier diodes are shown in Fig. 9. The RE:ZrO_2 based SBDs exhibit better rectification behavior, when compared to the undoped ZrO_2 based SBD. The calculated values of diode parameters (J_S, Φ_B, n, and R_S) are presented in Table 4. The ideality factor (n) is equal to one for the ideal Schottky diode. But, the fabricated SBDs exhibit a higher value of n, which is owing to the distribution of interface states, series resistance, and the voltage drop

Journal Pre-proof

Journal Pre-proof

across the ZrO_2 insulating layer [50]. However, the RE:ZrO_2 based SBDs show a better n value than undoped ZrO_2 SBD (n = 3.24). The values are 2.71, 2.48, and 2.64 for the Ce:ZrO_2, Gd:ZrO_2, and Y:ZrO_2 based SBDs, respectively. Due to smaller crystallites in the Gd:ZrO_2 layer, the series resistance, inhomogeneities, and non-uniform distribution of the interfacial charges are decreased, which results in the improvement of the ideality factor of Al/Gd:ZrO_2/p-Si SBD [25].

It is observed that the saturation current density (J_S) increases with the increase of reverse bias in the SBDs, which is attributed to the presence of insulating layer between the metal and semiconductor, inhomogeneity of the barrier height, and image force effect [8,51]. The series resistance (R_S) is determined from the slope of the straight line of dV/dln(J) vs. J plot, as shown in Fig. 11. For the Al/undoped ZrO_2/p-Si SBD, the saturation current density (J_S) and series resistance (R_S) values are 6.494×10^{-12} A/cm^2 and 282 kΩ, respectively (Table 4). The lower J_S value is attributed to the rod-shaped grains present in the undoped ZrO_2 film. But, the RE:ZrO_2 based SBDs show an increment in the reverse current density. Particularly, the Al/Gd:ZrO_2/p-Si SBD exhibits a higher J_S value of 1.313×10^{-10} A/cm^2 with a lower R_S value of 215 kΩ. Due to the larger ionic radius of Gd^{3+}, the crystallite size is reduced in the Gd:ZrO_2 film. This leads to an increase of defects like oxygen vacancies and dislocations, which in turn, increase the microstrain in the lattice. For the Gd:ZrO_2 film, the values of δ and ε are found to be 4.643×10^{16} and 7.386×10^{-3}, respectively. During the annealing treatment, the crystallites agglomerate and lead to the larger square-shaped grains. The defects segregated at grain boundaries can trap the charge carriers and increase the reverse current density by providing the percolation path for charge transport [52,53]. Since, the current flow is restricted by pores and micro-cracks present in the Y:ZrO_2 film, the grains connected by grain boundaries facilitate the reverse current. When compared to the Gd:ZrO_2 and Y:ZrO_2 based SBDs, the reverse current density decreases in the Ce:ZrO_2 based SBD, because of the smooth surface.

The value of Φ_B is calculated to be 1.04 eV for the Al/undoped ZrO_2/p-Si SBD and the Φ_B changes with respect to the RE dopants. Schottky barrier diodes fabricated with the insulating layers of Ce:ZrO_2, Gd:ZrO_2, and Y:ZrO_2 exhibit the Φ_B values of 0.99 eV, 0.94 eV, and 0.97 eV, respectively. It is obvious that the Φ_B decreases with a reduction in crystallite size associated with large defects. When compared to the Ce:ZrO_2 based SBD, the Φ_B is lower for the Gd:ZrO_2 and Y:ZrO_2 based SBDs. This is because the carrier concentration increases due to the oxygen vacancies created by Gd^{3+} and Y^{3+} ions in the Zr-O lattice [54]. In Fig.12, the I-V characteristics

show that the turn-on voltage is improved for the RE:ZrO_2 based SBDs. A turn-on voltage of 0.4 V is noticed for the Al/Gd:ZrO_2/p-Si SBD due to the lower barrier height [55].

4. Conclusion

In summary, the rare earth (8wt.% of Ce, Gd, and Y) doped ZrO_2 thin films were prepared by spin-coating technique and the RE:ZrO_2 based MIS Schottky barrier diodes were fabricated. The XRD results reveal the monoclinic phase for the undoped ZrO_2 film and the crystallite size (D) is 6.752 nm. The partial tetragonal phase for the Gd:ZrO_2 and Y:ZrO_2 films is owing to the oxygen vacancies created in the ZrO_2 lattice. Moreover, the crystallite size decreases with the increase of the ionic radius of dopants. The smallest D value (4.640 nm) is obtained for the Gd:ZrO_2 film. The SEM analysis reveals the square-shaped grains for the Gd:ZrO_2 thin film, which is due to the agglomeration of smaller crystallites at 600 ^{o}C. The presence of Zr, O, Ce, Gd, and Y elements are confirmed by the EDX analysis. The band gap (E_g) is 5.64 eV for the undoped ZrO_2, and the value is reduced to 5.25 eV for the Gd:ZrO_2. The higher electrical conductivity ($\sigma_{dc} = 1.172 \times 10^{-11}$ S/cm) with the activation energy (E_a) of 0.068 eV is observed in the Gd:ZrO_2 thin film. This is owing to the increase of carrier concentration in the Zr-O lattice. The Al/RE:ZrO_2/p-Si SBDs exhibit an improved turn-on voltage. The calculated values of saturation current density (J_S), barrier height (Φ_B), and ideality factor (n) for the Al/undoped ZrO_2/p-Si SBD are 6.494×10^{-12} A/cm^2, 1.04 eV, and 3.24, respectively. The Al/Gd:ZrO_2/p-Si SBD exhibits the values of 1.313×10^{-10} A/cm^2, 0.94 eV, and 2.48. Besides, the series resistance (R_S) is 282 kΩ for the undoped ZrO_2 based SBD and the value is reduced to 215 kΩ for the Gd:ZrO_2 based SBD. These results indicate that the Al/Gd:ZrO_2/p-Si SBD can be useful for the high fast switching and optoelectronic devices.

Acknowledgment

The authors are thankful to the Department of Science and Technology-FIST (Project No.: SR/FST/COLLEGE-154/2013) for providing the instrument facilities at Sri Ramakrishna Engineering College, Coimbatore, India.

References

[1] M. Soylu, F. Yakuphanoglu, Photovoltaic and interface state density properties of the Au/n-GaAs Schottky barrier solar cell, Thin Solid Films, 519 (2011) 1950-1954.

Journal Pre-proof

[2] M. Ali, V. Cimalla, V. Lebedev, H. Romanus, V. Tilak, D. Merfeld, P. Sandvik, O. Ambacher, Pt/GaN Schottky diodes for hydrogen gas sensors, Sens. Actuators, B 113 (2006) 797-804.

[3] P.C. Chang, Y.K. Su, K.J. Lee, C.L. Yu, S.J. Chang, C.H. Liu, Improved performance of GaN-based Schottky barrier photodetectors by annealing Ir/Pt Schottky contact in O_2, J. Alloys Compd. 504S (2010) S429-S431.

[4] A. Maestrini, B. Thomas, H. Wang, C. Jung, J. Treuttel, Y. Jin, G. Chattopadhyay, I. Mehdi, G. Beaudin, Schottky diode-based terahertz frequency multipliers and mixers, C. R. Phys. 11 (2010) 480-495.

[5] R. Islam, G. Shine, K.C. Saraswat, Schottky barrier height reduction for holes by Fermi level depinning using metal/nickel oxide/silicon contacts, Appl. Phys. Lett. 105 (2014) 182103.

[6] C.-Y. Li, M.-Y. Cheng, M.-P. Houng, C.-F. Yang, J. Liu, Electric Characteristic Enhancement of an AZO/Si Schottky Barrier Diode with Hydrogen Plasma Surface Treatment and Al_xO_x Guard Ring Structure, Materials, 11 (2018) 90.

[7] P.R.S. Reddy, V. Janardhanam, I. Jyothi, H.S. Chang, S.N. Lee, M.S. Lee, V.R. Reddy, C.J. Choi, Microstructural and electrical properties of Al/n-type Si Schottky diodes with Au-CuPc nanocomposite films as interlayer, Superlattices Microstruct. 111 (2017) 506-517.

[8] A. Tataroğlu, Ş. Altındal, Analysis of interface states and series resistance of MIS Schottky diodes using the current-voltage (I-V) characteristics, Microelectron. Eng. 85 (2008) 233-237.

[9] Y.C. Chan, J. Yu, D. Ho, Morphology, stoichiometry, and crystal structure control via post-annealing for Pt-ZnO nanograin Schottky barrier interfaces, Appl. Surf. Sci. 443 (2018) 506-514.

[10] V. Balasubramani, J. Chandrasekaran, R. Marnadu, P. Vivek, S. Maruthamuthu, S. Rajesh, Impact of Annealing Temperature on Spin Coated V_2O_5 Thin Films as Interfacial Layer in Cu/V_2O_5/n-Si Structured Schottky Barrier Diodes, J. Inorg. Organomet. Polym. Mater. 29 (2019) 1533-1547.

[11] R. Marnadu, J. Chandrasekaran, M. Raja, M. Balaji, V. Balasubramani, Impact of Zr content on multiphase zirconium–tungsten oxide (Zr-WOx) films and its MIS structure of

Journal Pre-proof

Cu/Zr-WOx/p-Si Schottky barrier diodes, J. Mater. Sci.: Mater. Electron. 29 (2018) 2618-2627.

[12] Y. Caglar, M. Caglar, S. Ilican, XRD, SEM, XPS studies of Sb doped ZnO films and electrical properties of its based Schottky diodes, Optik (Munich, Ger.) 164 (2018) 424-432.

[13] Y.Z. Li, X.M. Li, X.D. Gao, Effects of post-annealing on Schottky contacts of Pt/ZnO films toward UV photodetector, J. Alloys Compd. 509 (2011) 7193-7197.

[14] Y. Liu, W.M. Tang, P.T. Lai, A comparative study of Hf and Ta incorporations in the dielectric of Pd-WO_3-SiC Schottky-diode hydrogen sensor, Sens. Actuators, B 259 (2018) 725-729.

[15] H. Elhouichet, W.B.H. Othmen, S. Dabboussi, Effect of Sb, Tb^{3+} Doping on Optical and Electrical Performances of SnO_2 and Si Based Schottky Diodes, Silicon (2019) 10.1007/s12633-019-00164-y.

[16] B.S. Mwankemwa, M.J. Legodi, M. Mlambo, J.M. Nel, M. Diale, Structural, morphological, optical and electrical properties of Schottky diodes based on CBD deposited ZnO:Cu nanorods, Superlattices Microstruct. 107 (2017) 163-171.

[17] C.C. Chew, K.H. Goh, M.S. Gorji, C.G. Tan, S. Ramesh, Y.H. Wong, Breakdown field enhancement of Si-based MOS capacitor by post-deposition annealing of the reactive sputtered ZrO_xN_y gate oxide, Appl. Phys. A: Mater. Sci. Process. 122 (2016) 66.

[18] S. Chang, R. Doong, The Effect of Chemical States of Dopants on the Microstructures and Band Gaps of Metal-Doped ZrO_2 Thin Films at Different Temperatures, J. Phys. Chem. B 108 (2004) 18098-18103.

[19] L. Liang, R. Chen, Z. Mo, Color tunable up-conversion emission of ZrO_2:Yb^{3+}, Er^{3+} thin films prepared by chemical solution deposition, Ceram. Int. 44 (2018) 19661-19664.

[20] S.M. Hwang, J.H. Choi, S.M. Lee, J.H. Lim, J. Joo, Phase Transition and Microstructural Changes of Sol-Gel Derived ZrO_2/Si Films by Thermal Annealing: Possible Stability of Tetragonal Phase without Transition to Monoclinic Phase, J. Phys. Chem. C 116 (2012) 11386-11392.

[21] R.R. Gonçalves, J.J. Guimarães, J.L. Ferrari, L.J.Q. Maia, S.J.L. Ribeiro, Active planar waveguides based on sol-gel Er^{3+}-doped SiO_2-ZrO_2 for photonic applications:

Journal Pre-proof

Journal Pre-proof

Morphological, structural and optical properties, J. Non-Cryst. Solids 354 (2008) 4846-4851.

[22] H.J.A. Yadav, B. Eraiah, H. Nagabhushana, R.B. Basavaraj, N.H. Deepthi, Dy^{3+} doped cubic zirconia nanostructures prepared via ultrasound route for display applications, AIP Conf. Proc. 1832 (2017) 050115.

[23] G. Cabello, L. Lillo, C. Caro, B. Chornik, M.A. Soto, R. del Río, M. Tejos, Preparation and characterization of ZrO_2:Sm amorphous thin films by solid state photochemical deposition method, J. Phys. Chem. Solids 71 (2010) 1367-1372.

[24] S. Das, C.-Y. Yang, C.-H. Lu, Structural and Optical Properties of Tunable Warm-White Light-Emitting ZrO2:Dy^{3+}-Eu^{3+} Nanocrystals, J. Am. Ceram. Soc. 96 (2013) 1602-1609.

[25] K. Sasikumar, R. Bharathikannan, J. Chandrasekaran, M. Raja, Effect of Organic Additives on the Characteristics of Al/Organic Additive:ZrO_2/p-Si Metal-Insulator-Semiconductor (MIS) Type Schottky Barrier Diodes, J. Inorg. Organomet. Polym. Mater. (2019) https://doi.org/10.1007/s10904-019-01216-x.

[26] W.F. Lim, H.J. Quah, Q. Lu, Y. Mu, W.A.W. Ismail, B.A. Rahim, S.R. Esa, Y.Y. Kee, C.Z. Zhao, Z. Hassan, K.Y. Cheong, Effects of rapid thermal annealing on structural, chemical, and electrical characteristics of atomic-layer deposited lanthanum doped zirconium dioxide thin film on 4H-SiC substrate, Appl. Surf. Sci. 365 (2016) 296-305.

[27] D. Shikha, V. Mehta, S.C. Sood, J. Sharma, Structural and optical properties of ZnO thin films deposited by sol-gel method: effect of stabilizer concentration, J. Mater. Sci.: Mater. Electron. 26 (2015) 4902-4907.

[28] C.-H. Liu, P.-C. Juan, Y.-H. Chou, H.-W. Hsu, The effect of lanthanum (La) incorporation in ultra-thin ZrO_2 high-k gate dielectrics, Microelectron. Eng. 89 (2012) 2-5.

[29] D.Q. Xiao, G. He, J.G. Lv, P.H. Wang, M. Liu, J. Gao, P. Jin, S.S. Jiang, W.D. Li, Z.Q. Sun, Interfacial modulation and electrical properties improvement of solution-processed ZrO_2 gate dielectrics upon Gd incorporation, J. Alloys Compd. 699 (2017) 415-420.

[30] M.S. Lee, C.-H. An, K. Park, J.-Y. Choi, H. Kim, Effect of Y, Gd, Dy, and Ce Doping on the Microstructural and Electrical Properties of Sol-Gel-Deposited ZrO_2 Film, J. Electrochem. Soc. 158 (6) (2011) G133-G136.

Journal Pre-proof

Journal Pre-proof

[31] W.-C. Chen, Y.-J. Lin, Y.-H. Chen, H.-C. Chang, Effects of oxygen deficiency in the sol-gel ZrO_x film on the electrical properties of Au/ZrO_x/n-type Si/In devices, Semicond. Sci. Technol. 25 (2010) 055003.

[32] C. Suryanarayana, M.G. Norton, X-ray diffraction: A practical approach, Plenum Press, New York, 1998.

[33] S.M. Mosavi, H. Kafashan, Physical properties of Cd-doped ZnS thin films, Superlattices Microstruct. 126 (2019) 139-149.

[34] G.K. Williamson, R.E. Smallman, Philos. Mag. 1 (1956) 34-46.

[35] Y.W. Zhang, Y. Yang, S. Jin, C.S. Liao, C.H. Yan, Doping effect on the grain size and microstrain in the sol-gel-derived rare earth stabilized zirconia nanocrystalline thin films, J. Mater. Sci. Lett. 21 (2002) 943-946.

[36] D. Arora, K. Asokan, A. Mahajan, H. Kaura, D.P. Singh, Structural, optical and magnetic properties of Sm doped ZnO at dilute concentrations, RSC Adv. 6 (2016) 78122-78131.

[37] P. Li, I.-W. Chen, J.E. Penner-Hahn, Effect of Dopants on Zirconia Stabilization-An X-ray Absorption Study: I, Trivalent Dopants, J. Am. Ceram. Soc. 77 (1994) 118-128.

[38] S. Salari, F.E. Ghodsi, A significant enhancement in the photoluminescence emission of the Mg doped ZrO_2 thin films by tailoring the effect of oxygen vacancy, J. Lumin. 182 (2017) 289-299.

[39] F.E. Ghodsi, J. Mazloom, Optical, electrical and morphological properties of p-type Mn-doped SnO_2 nanostructured thin films prepared by sol-gel Process, Appl. Phys. A: Mater. Sci. Process. 108 (2012) 693-700.

[40] J. Tauc, R. Grigorovici, A. Vancu, Optical Properties and Electronic Structure of Amorphous Germanium, Phys. Status Solidi B 15 (1966) 627-637.

[41] J. Chen, D. Chen, J. He, S. Zhang, Z. Chen, The microstructure, optical, and electrical properties of sol-gel-derived Sc-doped and Al-Sc co-doped ZnO thin films, Appl. Surf. Sci. 255 (2009) 9413-9419.

[42] V.S. Anitha, S.S. Lekshmy, K. Joy, Effect of Mn doping on the Structural, Magnetic, Optical and Electrical properties of ZrO_2-SnO_2 thin films prepared by sol-gel method, J. Alloys Compd. 675 (2016) 331-340.

Journal Pre-proof

[43] M. Balaji, J. Chandrasekaran, M. Raja, Role of substrate temperature on MoO_3 thin films by the JNS pyrolysis technique for P-N junction diode application, Mater. Sci. Semicond. Process. 43 (2016) 104-113.

[44] A.K. Jonsson, G.A. Niklasson, M. Veszelei, Electrical properties of ZrO_2 thin films, Thin Solid Films 402 (2002) 242-247.

[45] M.-T. Wang, S.-Y. Deng, T.-H. Wang, B.Y. Cheng, J.Y. Lee, The Ohmic Conduction Mechanism in High-Dielectric-Constant ZrO_2 Thin Films, J. Electrochem. Soc. 152 (2005) G542-G544.

[46] K. Apriany, I. Permadani, D.G. Syarif, S. Soepriyanto, F. Rahmawati, Electrical conductivity of zirconia and yttrium-doped zirconia from Indonesian local zircon as prospective material for fuel cells, IOP Conf. Ser. Mater. Sci. Eng. 107 (2016) 012023.

[47] Q.X. Jia, K. Ebihara, T. Ikegami, W.A. Anderson, Metal/TaN (~5 nm)/Si Diode Fabricated by DC Magnetron Sputtering, Appl. Phys. A: Mater. Sci. Process. 58 (1994) 487-491.

[48] K.R. Peta, B.-G. Park, S.-T. Lee, M.-D. Kim, J.-E. Oh, Temperature-dependent electrical properties of (Pt/Au)/Ga-polarity GaN/Si(111) Schottky diode, Microelectron. Eng. 93 (2012) 100-104.

[49] S.K. Cheung, N.W. Cheung, Extraction of Schottky diode parameters from forward current-voltage characteristics, Appl. Phys. Lett. 49 (1986) 85-87.

[50] H.-K. Lee, I. Jyothi, V. Janardhanam, K.-H. Shim, H.-J. Yun, S.-N. Lee, H. Hong, J.-C. Jeong, C.-J. Choi, Effects of Ta-oxide interlayer on the Schottky barrier parameters of Ni/n-type Ge Schottky barrier diode, Microelectron. Eng. 163 (2016) 26-31.

[51] E.H. Rhoderick, R.H. Williams, Metal-Semiconductor Contacts, second ed., Clarendon Press, Oxford, 1988.

[52] C. Lv, C. Zhu, C. Wang, D. Li, X. Ma, D. Yang, Defect-related electroluminescence from metal-oxide-semiconductor devices with ZrO_2 films on silicon, Superlattices Microstruct. 99 (2016) 186-191.

[53] M. Kasu, T. Oshima, K. Hanada, T. Moribayashi, A. Hashiguchi, T. Oishi, K. Koshi, K. Sasaki, A. Kuramata, O. Ueda, Crystal defects observed by the etch-pit method and their effects on Schottky-barrier-diode characteristics on $(\bar{2}01)$ β-Ga_2O_3, Jpn. J. Appl. Phys. 56 (2017) 091101.

Journal Pre-proof

[54] T. Han, Y. Shi, H. Wu, C. Liu, Fabrication and characterization of aluminum-doped zinc oxide Schottky diodes on n-GaN, Curr. Appl. Phys. 12 (2012) 1536-1540.

[55] M. Das, J. Datta, A. Dey, R. Jana, A. Layek, S. Middya, P.P. Ray, One step hydrothermal synthesis of a rGO-TiO_2 nanocomposite and its application on a Schottky diode: improvement in device performance and transport properties, RSC Adv. 5 (2015) 101582-101592.

Journal Pre-proof

Figure captions

Fig. 1 Schematic diagram of the Al/RE:ZrO_2/p-Si SBD

Fig. 2 XRD patterns of the undoped ZrO_2 and RE:ZrO_2 thin films coated on Si (100) substrates

Fig. 3 SEM images of the (a) undoped ZrO_2 (b) Ce:ZrO_2 (c) Gd:ZrO_2 (d) Y:ZrO_2 thin films

Fig. 4 EDX spectra of the (a) undoped ZrO_2 (b) Ce:ZrO_2 (c) Gd:ZrO_2 (d) Y:ZrO_2 thin films

Fig. 5 Transmittance spectra of the undoped ZrO_2 and RE:ZrO_2 thin films

Fig. 6 Tauc plots of the undoped ZrO_2 and RE:ZrO_2 thin films

Fig. 7 dc electrical conductivity of the undoped ZrO_2 and RE:ZrO_2 thin films

Fig. 8 Plot of $\ln(\sigma_{dc})$ vs. 1/T for the undoped ZrO_2 and RE:ZrO_2 thin films

Fig. 9 ln(J)-V characteristics of the RE:ZrO_2 (RE = Ce, Gd, and Y) based MIS type SBDs

Fig. 10 Energy band diagram of the Al/RE:ZrO_2/p-Si SBD, Φ_M and Φ_{Si} are the work functions of Al and p-Si ($\Phi_M < \Phi_{Si}$), Φ_B is the barrier height, χ_S is the semiconductor electron affinity, qV_i (= Φ_{Si}-Φ_M) is the built-in potential

Fig. 11 dV/d(lnJ) vs. J plot of the RE:ZrO_2 (RE = Ce, Gd, and Y) based MIS type SBDs

Fig. 12 I-V characteristics of the RE:ZrO_2 (RE = Ce, Gd, and Y) based MIS type SBDs

Table captions

Table 1 Structural parameters of the undoped ZrO_2 and RE:ZrO_2 thin films

Table 2 Band gaps of the undoped ZrO_2 and RE:ZrO_2 thin films

Table 3 dc electrical parameters of the undoped ZrO_2 and RE:ZrO_2 thin films

Table 4 Diode parameters of the RE:ZrO_2 (RE = Ce, Gd, and Y) based MIS type SBDs

Journal Pre-proof

Table 1

Thin film	**Diffraction angle (2θ)**	**(h k l)**	**Interplanar spacing (d) Å**	**FWHM (β) rad**	**Crystallite size (D) nm**	**Dislocation density (δ) $\times 10^{16}$ lines/m^2**	**Micro strain (ε) $\times 10^{-3}$ lines/m^2**	**Stacking fault (SF) $\times 10^{-3}$**
undoped ZrO_2	31.22	(1 1 1)	2.863	0.0210	6.752	2.193	5.076	12.468
Ce:ZrO_2	31.18	(1 1 1)	2.866	0.0243	5.842	2.929	5.866	14.399
Gd:ZrO_2	31.06	(1 1 1)	2.877	0.0306	4.640	4.643	7.386	18.078
Y:ZrO_2	31.11	(1 1 1)	2.873	0.0246	5.775	2.998	5.935	14.542

Journal Pre-proof

Table 2

Thin film	Thickness (nm)	Band gap energy E_g (eV)
undoped ZrO_2	364	5.64
$Ce:ZrO_2$	382	5.53
$Gd:ZrO_2$	376	5.25
$Y:ZrO_2$	385	5.38

Journal Pre-proof

Journal Pre-proof

Table 3

Thin film	**Conductivity σ_{dc} (S/cm)**	**Activation Energy E_a (eV)**
undoped ZrO_2	5.827×10^{-12}	0.093
Ce:ZrO_2	8.038×10^{-12}	0.073
Gd:ZrO_2	1.172×10^{-11}	0.068
Y:ZrO_2	9.572×10^{-12}	0.071

Journal Pre-proof

Schottky barrier diode	**Reverse saturation current density J_S (A/cm^2)**	**Barrier height Φ_B (eV)**	**Series resistance R_S (kΩ)**	**Ideality factor n**
Al/undoped ZrO_2/p-Si	6.494×10^{-12}	1.04	282	3.24
Al/Ce:ZrO_2/p-Si	1.768×10^{-11}	0.99	270	2.71
Al/Gd:ZrO_2/p-Si	1.313×10^{-10}	0.94	215	2.48
Al/Y:ZrO_2/p-Si	3.576×10^{-11}	0.97	238	2.64

Table 4

Journal Pre-proof

Journal Pre-proof

Fig. 1

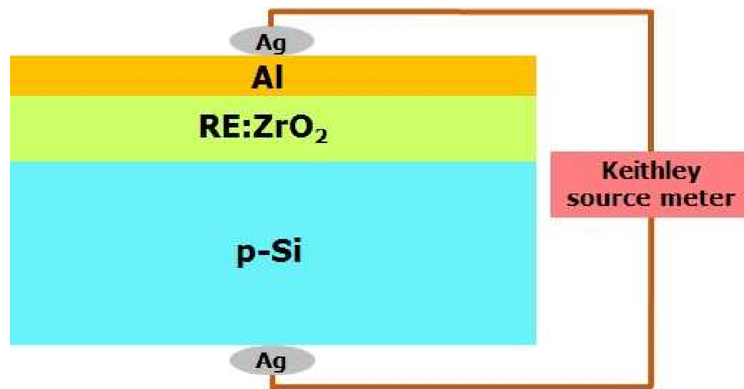

Journal Pre-proof

Fig. 2

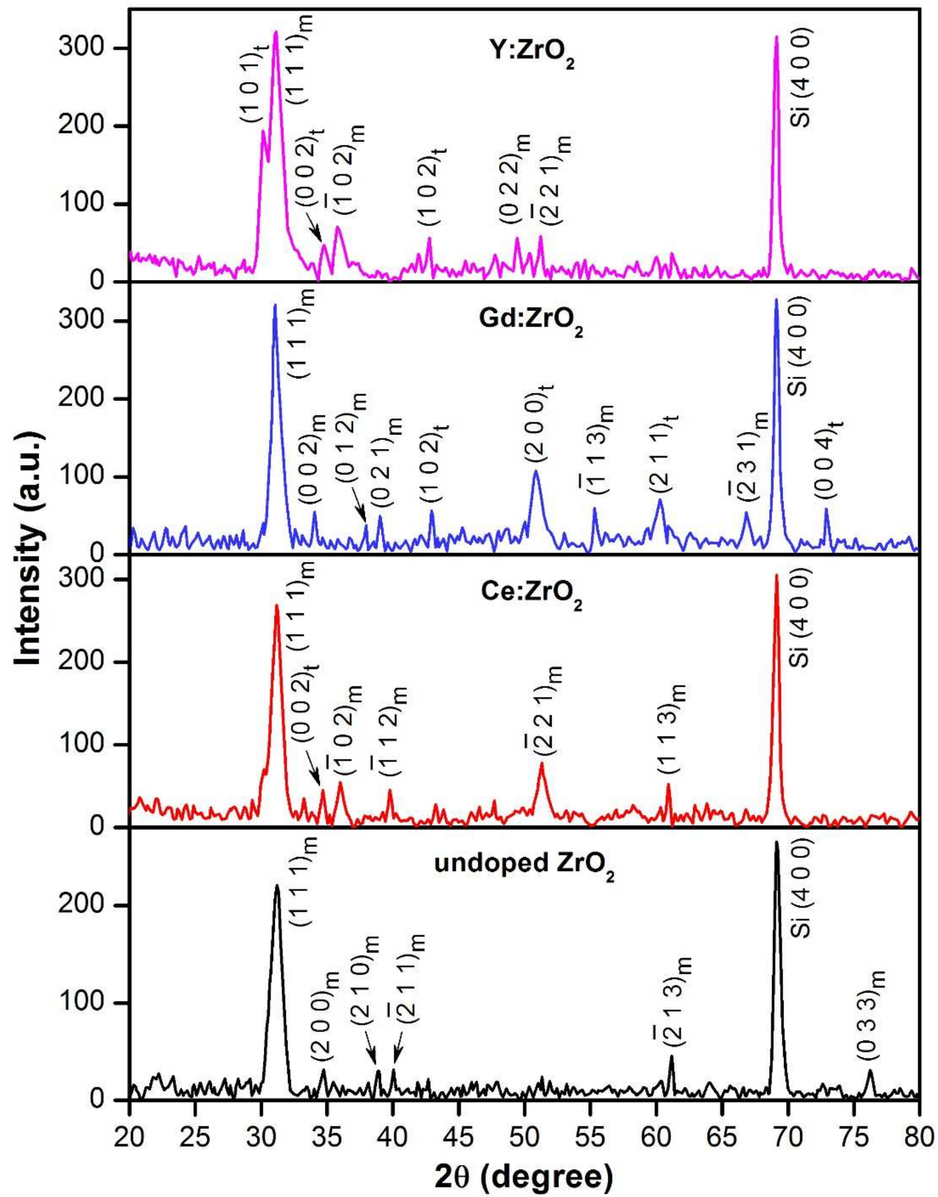

Fig. 3

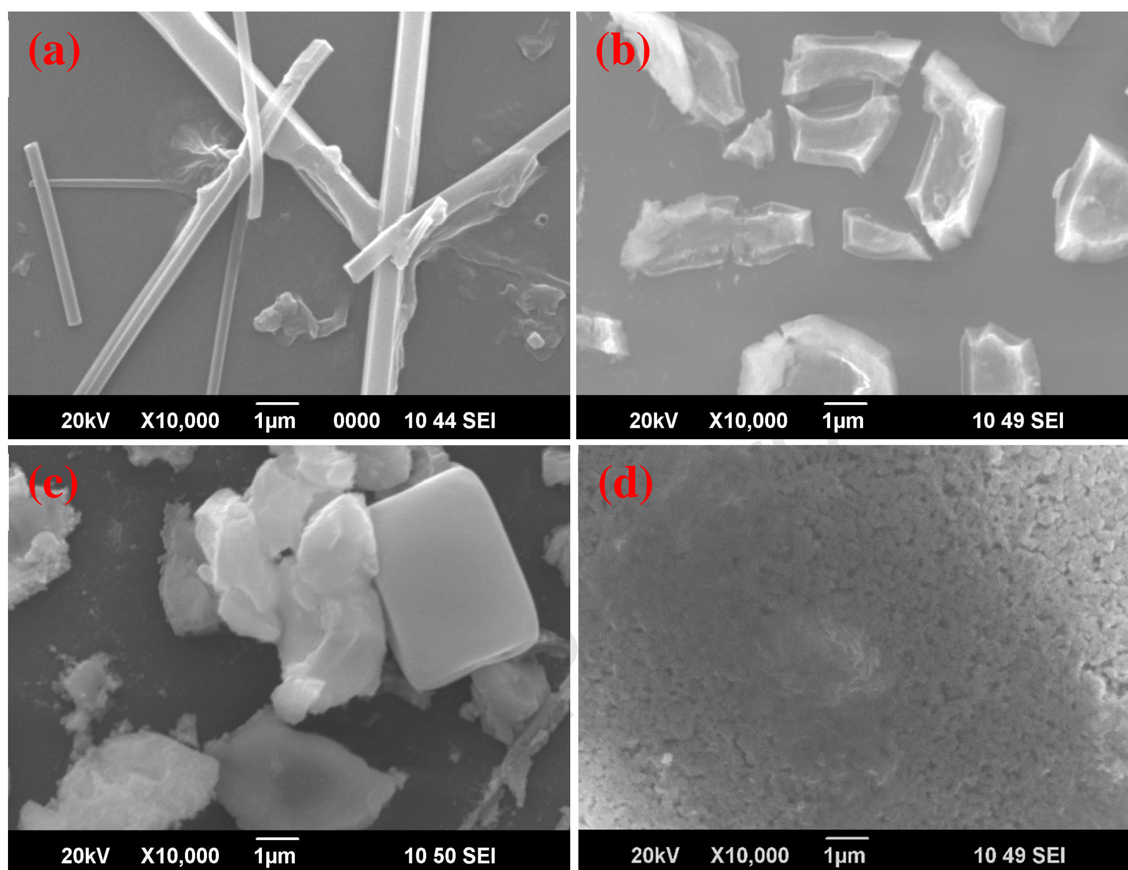

Fig. 4

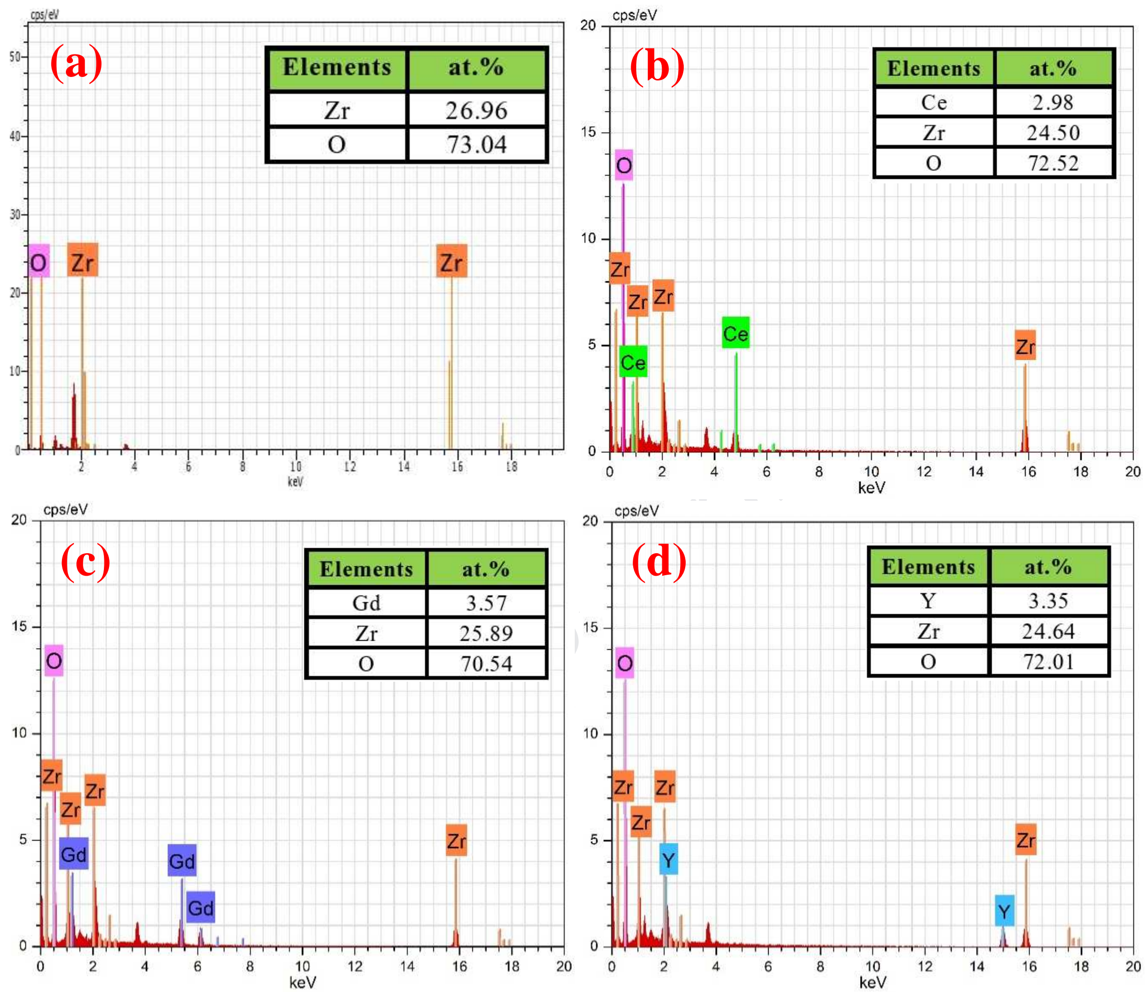

Fig. 5

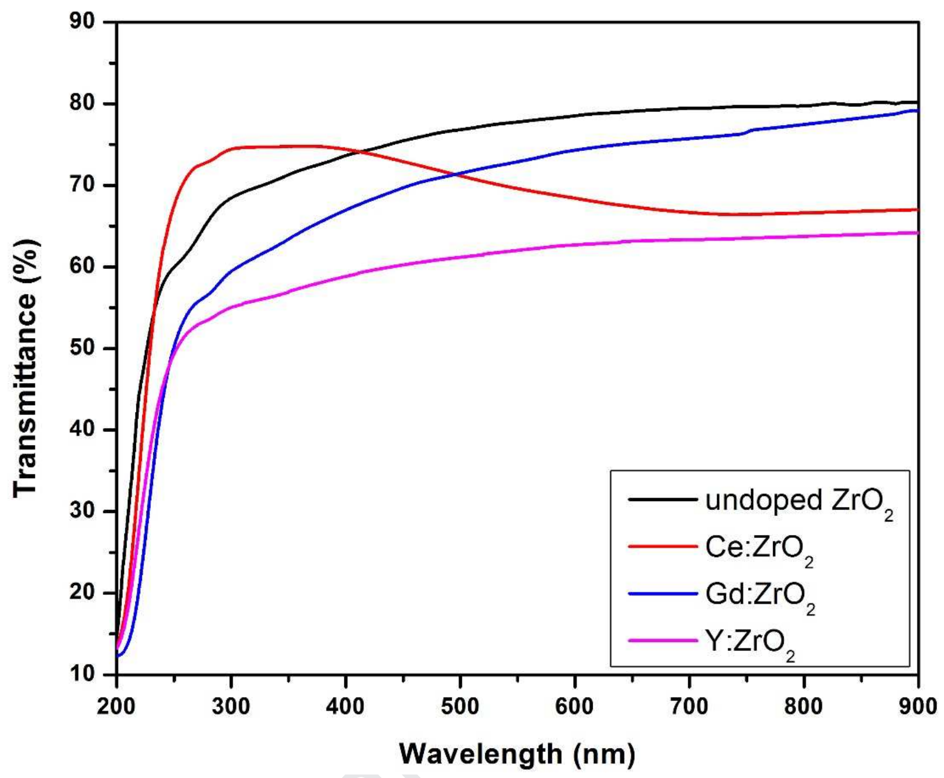

Journal

Fig. 6

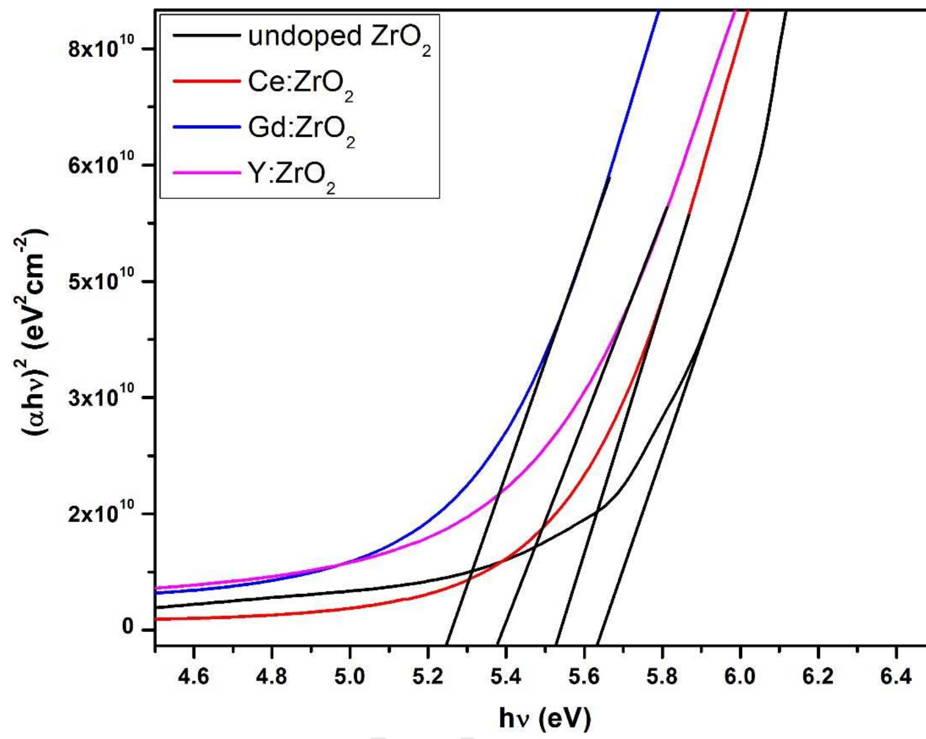

Journal

Journal Pre-proof

Fig. 7

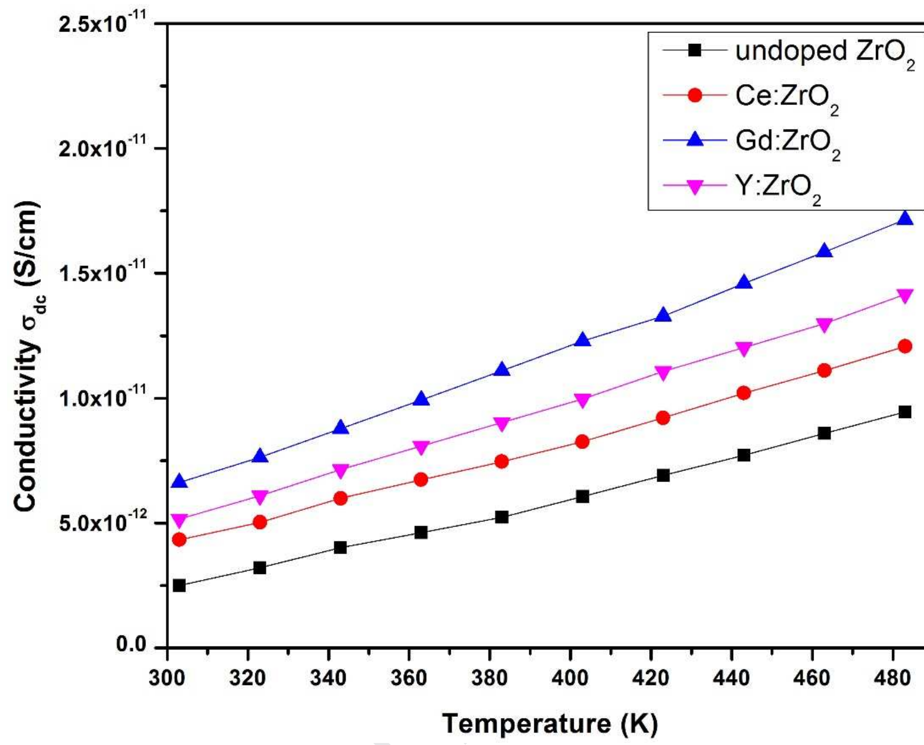

Fig. 8

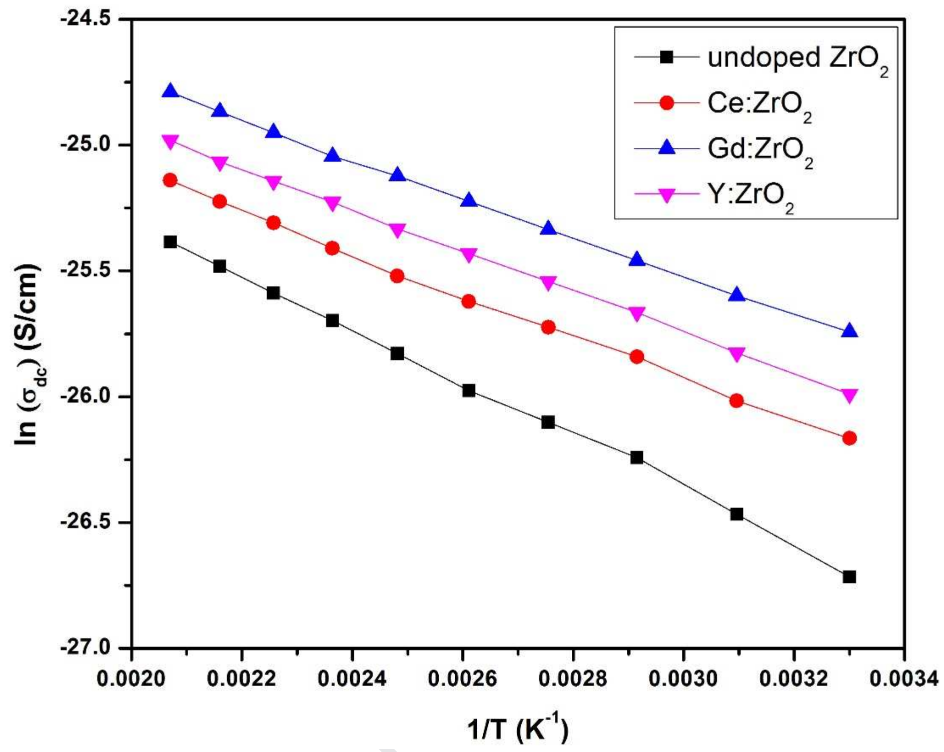

Journal

Fig. 9

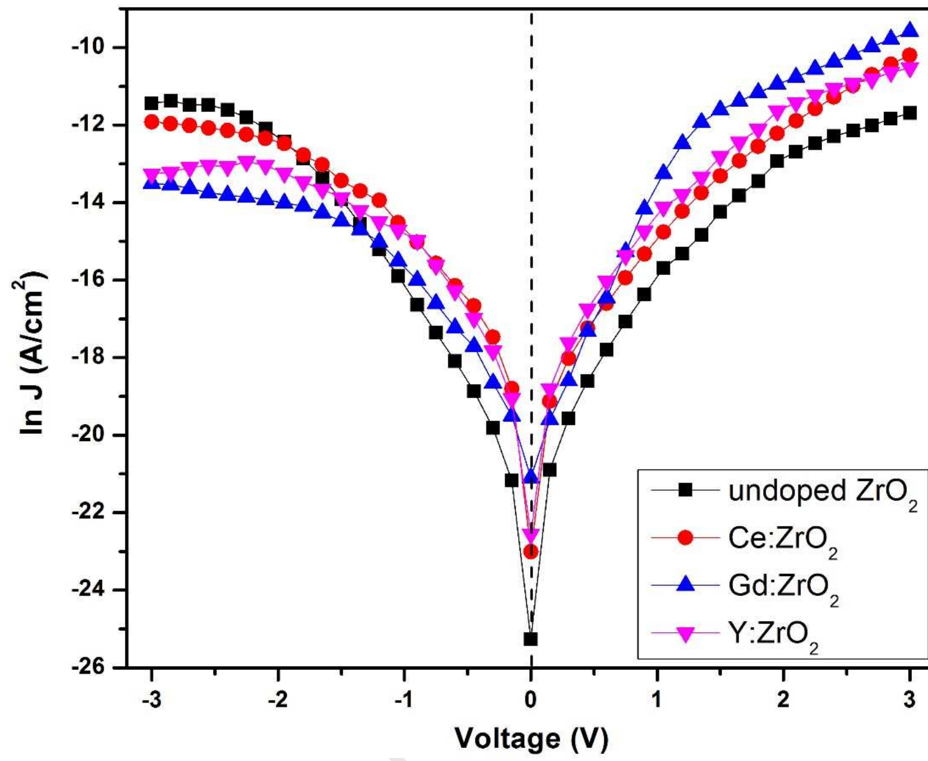

Journal

Journal Pre-proof

Fig. 10

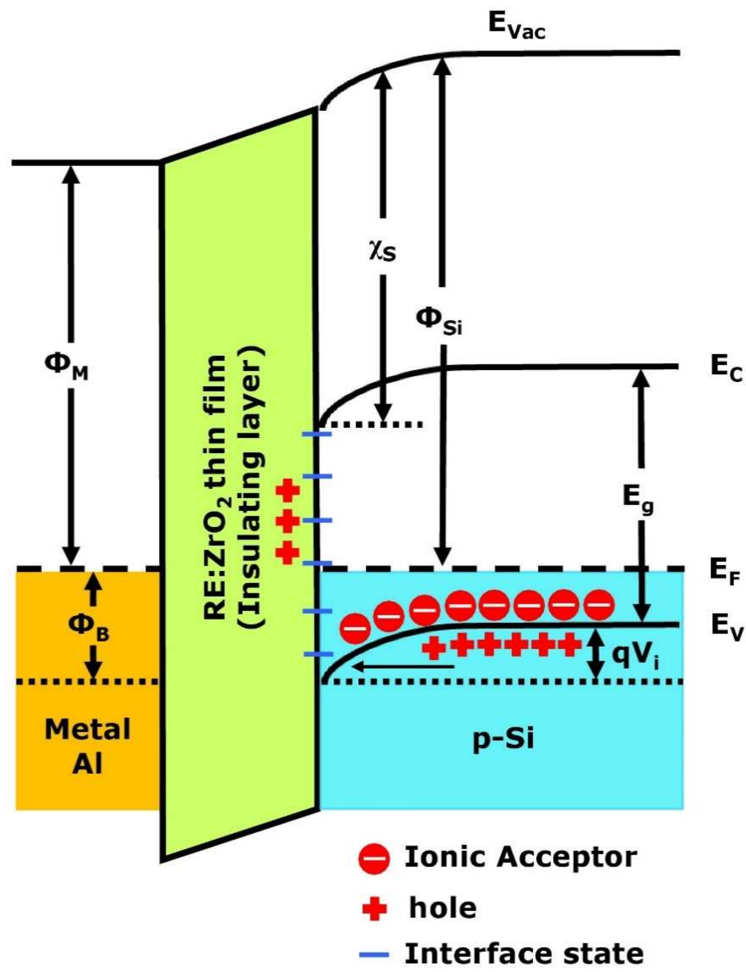

Fig. 11

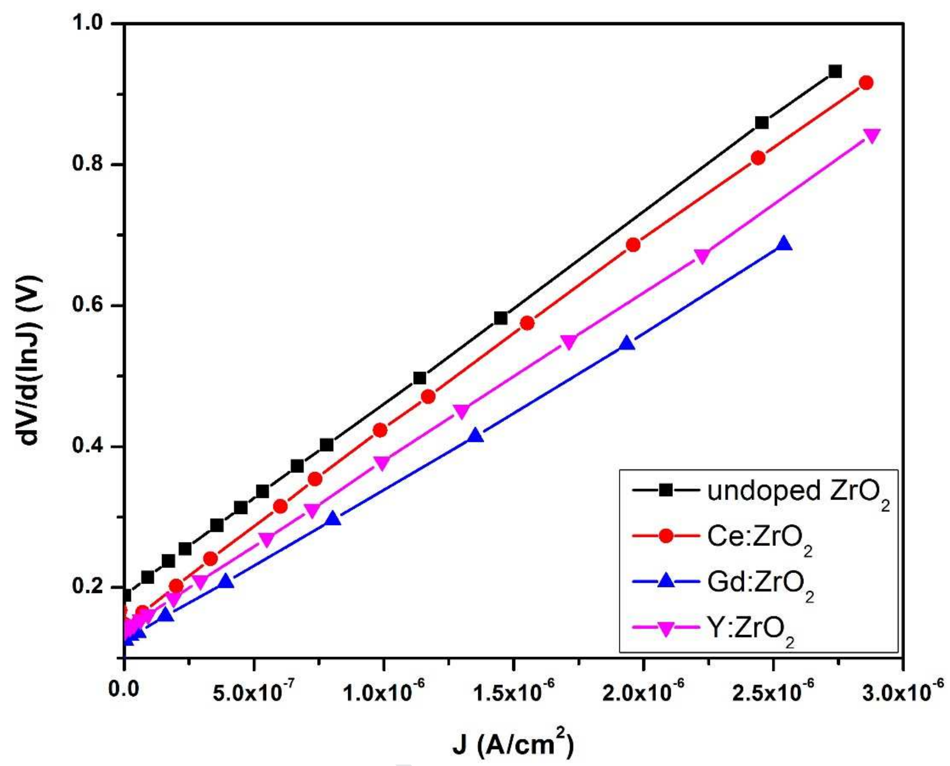

Journal

Fig. 12

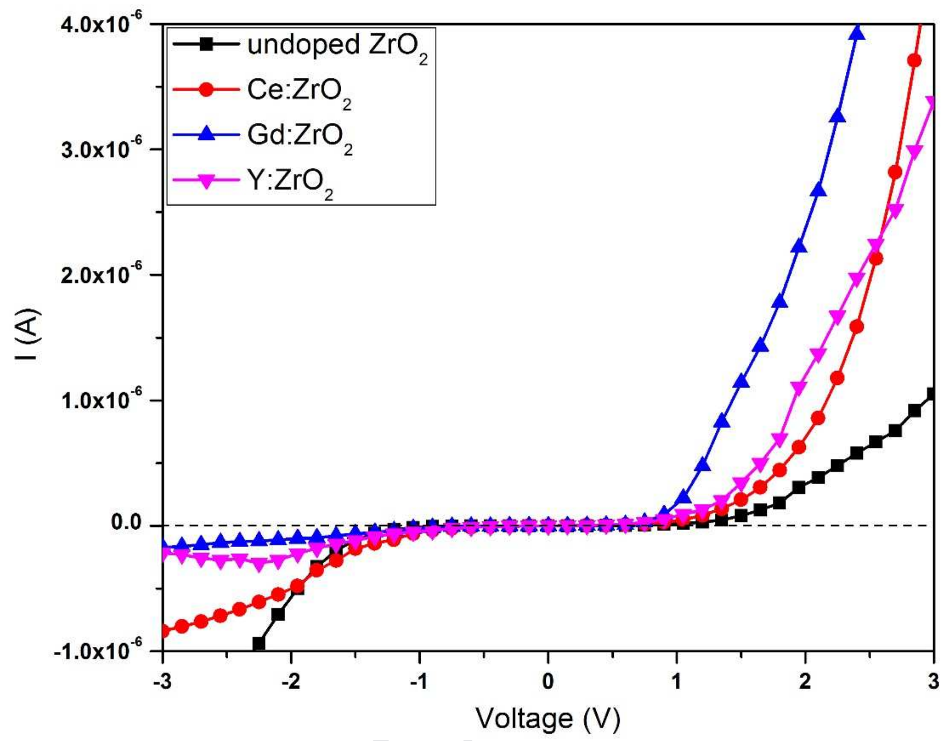

Journal

Highlights

- Rare earth (Ce, Gd, and Y) doped ZrO_2 insulating layer based MIS type Schottky barrier diodes have been fabricated.
- The mixed phase of m-ZrO_2 and t-ZrO_2 is observed for the Gd:ZrO_2 thin film with the smaller crystallite size of 4.640 nm.
- In Gd:ZrO_2 film, the increase in reverse current density is owing to the presence of square-shaped grains with dislocations.
- A higher dc electrical conductivity (σ_{dc}) is observed for the Gd:ZrO_2 film.
- When compared to the Al/undoped ZrO_2/p-Si SBD, the Al/Gd:ZrO_2/p-Si SBD shows an improvement in the values of Φ_B, R_S, and n.

Journal Pre-proof

Journal Pre-proof

AUTHOR STATEMENT

Manuscript Title:

Fabrication and characterization of rare earth (Ce, Gd, and Y) doped ZrO_2 based metal-insulator-semiconductor (MIS) type Schottky barrier diodes

All persons who meet authorship criteria are listed as authors, and all authors certify that they have participated sufficiently in the work to take public responsibility for the content, including participation in the concept, design, analysis, writing, or revision of the manuscript. Furthermore, each author certifies that this material or similar material has not been and will not be submitted to or published in any other journal.

Credit statement:

K. Sasikumar: Conceptualization, Investigation, Writing - Original Draft; **R. Bharathikannan:** Supervision; **M. Raja:** Resources; **B. Mohanbabu:** Writing - Review & Editing;

Journal Pre-proof

Journal Pre-proof

DECLARATION OF INTERESTS

☒ The authors declare that they have no known competing financial interests or personal relationships that could have appeared to influence the work reported in this paper.

☐ The authors declare the following financial interests/personal relationships which may be considered as potential competing interests:

Declarations of interest: none

Journal Pre-proof